

The role of particulate morphology and chemistry on the nucleation and growth of water and ice in the exhaust plume

By M. Yazdani[†], T. Ferreira AND S. K. Lele

Contrails are known to be a major contributor to climate forcing (30–70% of aviation-induced radiative forcing), and emissions [nonvolatile particulate matter (nvPM)] are known to be the primary source of ice nucleation, which is the precursor of contrail formation. We aim to explore the frequently neglected role of soot particle morphology and chemistry on the kinetics of nucleation and the early stages of the post-nucleation growth mechanism. The findings of this research will enable a more rigorous prediction of contrail formation, especially as a function of fuel chemistry and resulting emission characteristics.

1. Introduction

Contrail cirrus is estimated to be the biggest aviation climate-forcing factor (Lee *et al.* 2021). They are formed as contrails — clouds of ice crystals from aircraft condensation trails — spread under certain conditions (e.g., high humidity) and eventually become indistinguishable from natural cirrus clouds (Minnis *et al.* 1998).

One of the key challenges with the formation of cirrus clouds is characterizing their evolution from soot — carbonaceous particles originated by incomplete combustion of fossil fuels and the main precursors — to ice crystals. Water and ice nucleation can occur by homogeneous or (different types of) heterogeneous nucleation. In addition, flow mixing and nucleation rates may have an impact on the number, size and morphology of subsequent ice crystals, which may alter the radiative effect of the contrail. The current modeling state of art either grossly simplifies the nucleation mechanism, ignoring the kinetics of nucleation altogether (e.g., Schumann 2012; Fritz 2022), or ignores the role of subtle mechanisms such as particulate morphology and surface energy on nucleation behavior. There are several research efforts focusing on the role that particulate characteristics play on their nucleation behavior [Vali *et al.* (2015) and references therein]. For example, the experimental study of Kulkarni *et al.* (2016), simulated several treatments to fresh soot particles representative of atmospheric processes that occur. They observed that the humidification of organic-coated particles was able to shift the type of nucleation.

Our research aims to study the role of particle morphology and surface energy (reflected in whether they are coated or uncoated) on their nucleation and post-nucleation behavior. The former is being studied through classical nucleation theory (CNT), considering the effect of particle fractal dimension on their surface energy; and the latter includes condensation and freezing on particles of different fractal dimensions. The key goal is to incite interest into further and more rigorous research in this area, so the conclusions presented here should be viewed with this in mind. The findings of this work could shed light into not only the ability to predict the role of these nuanced players

[†] RTX Technology Research Center

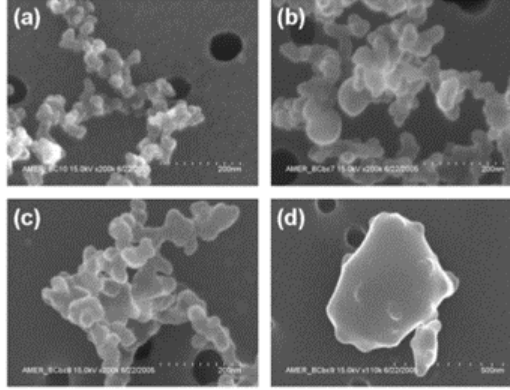


FIGURE 1. Scanning electron microscope (SEM) images of soot at different equivalence ratios: (a) $\phi = 2.3$, (b) $\phi = 2.8$, (c) $\phi = 3.5$ and (d) $\phi = 5.0$. Adopted from Slowik *et al.* (2007).

on the formation of ice crystals but also the derivation of relations between combustor architecture, fuels [e.g, Jet A vs. sustainable aviation fuel (SAF)] that affect the shape and chemistry of soot and the resulting ice crystal formation and growth. It also will enable a more rigorous prediction of secondary nucleation and formation of the cirrus cloud after the initial contrail is dissipated.

2. Problem statement

During the initial phases of contrail formation, nucleation and growth processes happen during the rapidly evolving mixing of the jet exhaust and atmospheric flow. Yet, the conditions in the mixing region are such that the kinetics of phase transformation could have comparable timescales to those of the flow. In addition, the particulates at which nucleation can occur are often highly fractal, as shown schematically in Figure 1. The role of particulate morphology in nucleation and growth processes is often neglected. One could argue that fractal particles enjoy a larger surface area compared to their spherical counterparts (with the same gyration radius), which could facilitate the nucleation process. The counterargument, however, could be that the highly fractal particles have less heterogeneity (often described as surface area-to-volume ratio), which could in turn hinder the nucleation affinity.

3. Approach

Figure 2 is a schematic illustration of possible pathways for a particulate to evolve as it goes through the mixing process. Nucleation on the particulate surface could be in the form of water nucleation or direct nucleation of ice (i.e., direct freezing), depending on the conditions of the surface (here a particle) and the ambient environment (details presented below). If water is nucleated, it undergoes the growth process, which is often referred to as condensation growth. Once enough energy is available, ice nucleation will occur within the droplet, followed by the growth of the ice crystal.

In order to represent the particle pathway (cooling rate) during the mixing process, a computational fluid dynamics (CFD) model of the exhaust plume with representative exit conditions (bypass ratio, temperature, water etc.) is used with a model of particle injection that represents particulate emission from the core exhaust. Figure 3 (top) shows

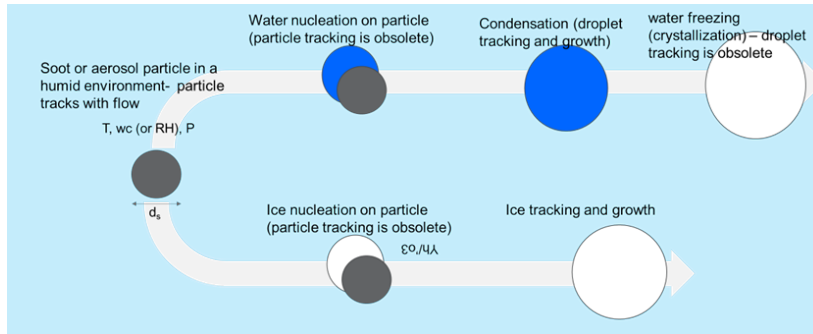


FIGURE 2. Schematic illustration of possible heterogeneous nucleation pathways.

example snapshots of the flow and particle field. Here, the particles change state (as described above) through what is being described as CNT. In this control case, particles are assumed to be spherical; therefore, it is only their size and chemistry that would drive the heterogeneous nucleation mechanism (in addition to the ambient conditions).

Individual particle trajectories extracted from this model are shown in Figure 3 (bottom). The goal is to extract sufficient samples of cooling rate for a range of initial conditions (jet exhaust flow mixing with the atmosphere), particle diameter, and supersaturation. The state of particles correspond to whether they are inactive (= 0) or activated by water (= 1) or by ice (= 2). The reference time t_0 on the plots on the right corresponds to the time of nucleation. The purpose of these plots is to illustrate the inherent delay associated with the nucleation process after the particle becomes supersaturated ($RH_i = 1.0$).

The physics-based approach presented here consists of employing CNT to capture the nucleation mechanism. The subsequent condensation of water as a result of nuclei growth in the supersaturated medium is simulated through interphase mass transfer across the water/gas interface. Supercooled crystallization is tracked through the phase-field method (PFM); the details of these steps are presented below.

3.1. Nucleation

The premise of the nucleation model presented here is based on the available free energy for phase transformation. That is, nucleation is only favorable when local free energy is sufficiently high for it to occur and for the nuclei to be sustained after formation. To that effect, nucleation is modeled through generalized CNT for water nucleation (condensation) and ice nucleation based on Noguera *et al.* (2006). The approach is based on a generalized form of the system's Gibb's free energy,

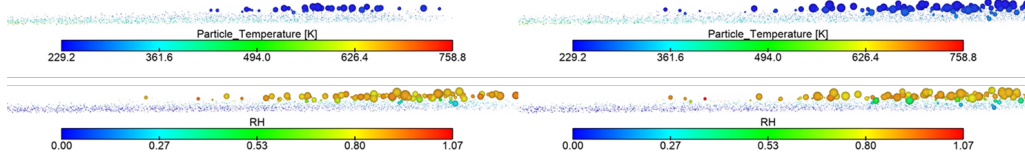
$$\Delta G = -nk_B T \ln S + \sigma (36 \pi v^2 \Phi(\theta))^{\frac{1}{3}} n^{\frac{2}{3}}. \quad (3.1)$$

The term S , in the first term on the right-hand side represents the system's entropy. For the nucleation of water (condensation), S takes the form

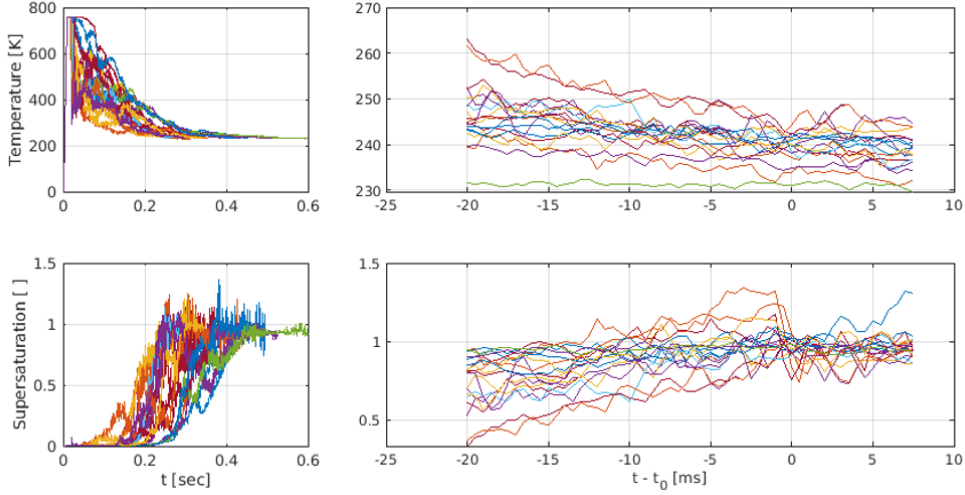
$$S = \Pi = P/P_0, \quad (3.2)$$

where P and P_0 , respectively, correspond to vapor pressure and saturation pressure for water. For the case of the nucleation of ice in supercooled liquid, we have

$$S = \exp\left(\frac{\Delta H_m}{k_B T_m^2} \Delta T\right). \quad (3.3)$$



(a)



(b)

FIGURE 3. An example snapshot of (top) the exhaust plume flow field and (bottom) sampled representation of possible paths particles would take along the exhaust plume as they enter the mixing region. t_0 represents the time at which a particle first encounters $RH_i = 1$.

The second term on the right-hand side of Eq. (3.1) represents the heterogeneity of the nucleation process and contains terms associated with surface energy. For the sake of brevity, we leave those details for a future report.

The conditions are favorable for nucleation when the available free energy from Eq. (3.1) overcomes the minimum energy barrier of nucleation (also referred to as critical free energy),

$$\Delta G^* = k_B T \frac{u}{\ln^2 S}, \quad u = \frac{16\pi\sigma^3 v^2 \Phi(\theta)}{3(k_B T)^3}. \quad (3.4)$$

Once this condition is met, the nucleation rate and the corresponding probability of nucleation can be calculated as:

$$F = F_0 \exp\left(-\frac{\Delta G^*}{k_B T}\right), \quad \tilde{P} = \frac{N_f}{N_0} = 1 - \exp\left(-\frac{dt}{dT} \int_{T_0}^T F dT\right) \quad (3.5)$$

The effect of particle morphology is reflected through nucleation volume and apparent surface energy of the particle as follows: in case of nucleation on a spherical particle, the nucleation volume is simply the geometric reduction of the particle volume from the critical nucleation volume,

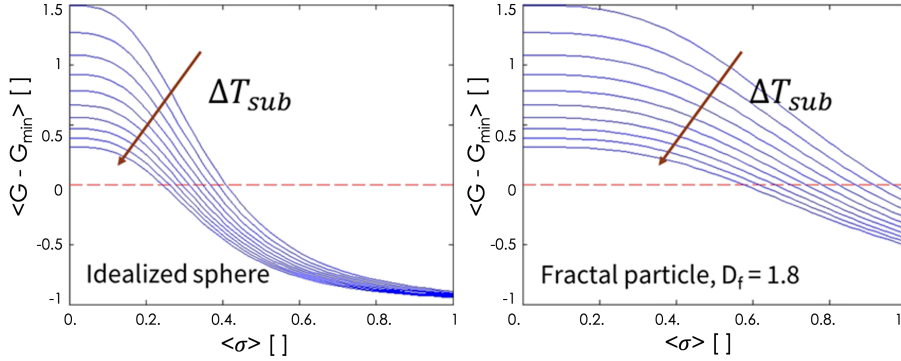


FIGURE 4. Notional example of how the proportion of a given particle with known fractal dimension and a nominal surface energy distribution would contribute to nucleation; a larger portion under the $G - G_{min} = 0$ threshold implies increased affinity to water.

$$v \approx r_c^3 - r_g^3; \quad r_c = \frac{2T_s\sigma}{\rho_l\Delta H\Delta T_{sub}}. \quad (3.6)$$

When nucleating on a fractal particle, the volume of the nuclei can be modified through radius of gyration of the particle as,

$$v \approx r_c^3 - \frac{1}{n_p} \left(\frac{r_g}{\bar{r}_p} \right)^{D_f}; \quad r_c = \frac{2T_s\sigma}{\rho_l\Delta H\Delta T_{sub}}; \quad \bar{r}_p = \frac{\sum_i r_{p,i}}{n_p}. \quad (3.7)$$

In addition, we can show, through arithmetic reduction, that the effective surface energy of a fractal particle can be defined as.

$$\sigma(\mathbf{x}) = \sigma_{ls,n} \left(\frac{r_g^3}{r_p^3(\mathbf{x}) (r_g - 2r_p(x))^3} \right)^{D_f}. \quad (3.8)$$

Figure 4 shows, notionally, the effect of particle morphology, $D_f = 1.8$ (fractal) vs. $D_f = 3$ (spherical), on the nucleation effectiveness (departure from minimum free energy) for a nominal distribution of surface energy (normalized by the mean surface energy of the particle). It shows that, for similar supercooling, the lower fractal dimension leads to an apparent reduction of the particle's propensity for nucleation, manifested by a higher overall energy difference against the energy barrier for the same surface energy.

3.2. Condensation

The formulation assumes that the distribution of vapor and liquid is computed based on the volume-of-fluid (VOF) approach, or on a similar front-tracking scheme. Therefore, note that the theoretical approach presented here is largely independent of the specific interface tracing scheme. Further details of the formulation presented in this section can be found in Yazdani *et al.* (2016). In summary, the continuity of each phase reflects the mass being transferred due to phase change,

$$\rho \nabla \cdot \mathbf{u} = -\dot{\rho} = f(j_e), \quad (3.9)$$

where j_e is the phase change mass flux (Hardt & Wondra 2008) according to the equation

$$j_e = \frac{h_{fg}^2}{\sqrt{2\pi R}} \frac{\rho_v}{T_{\text{sat}}^{3/2}} (T - T_{\text{sat}}), \quad (3.10)$$

where R is the universal gas constant, T_{sat} is the saturation temperature, and h_{fg} is the latent heat of evaporation.

3.3. Ice crystal growth

Supercooled crystallization in liquid is simulated through the PFM which is based on the minimization of free energy during phase transformation and has been extensively used to simulate the supercooled crystallization of metals and alloys (Karma 2001). The phase-field formulation is

$$\tau(n) \frac{\partial \Psi}{\partial t} = \nabla \cdot (\Gamma \nabla \Psi) + (\Psi - \lambda T (1 - \Psi^2)) (1 - \Psi^2). \quad (3.11)$$

More details about the specifics of the PFM and the terms in Eq. (3.11) above can be found in Yazdani *et al.* (2023); they are left out here for brevity.

In addition, note that this formulation has been extended to the so-called thin-film Stefan formulation of solidification, which allows the simulation of crystallization in supersaturated gas phase.

4. Results and discussion

4.1. Nucleation

Three fractal particles (shown at the top of Figure 5), generated through Raytheon Technologies Research Center's mesoscale soot post-nucleation model [which is an extension of Mitchell & Frenklach (1998)], were selected along with a spherical particle (as the control case). The schematic of particles undergoing nucleation is shown in Figure 3. Each particle has 50 trajectories available for the nucleation studies. The model tracks the time at which the particle becomes supersaturated (i.e., $t = t_0$) and a nucleation embryo is formed (i.e., $t = t_{nuc}$). The difference between these two time stamps represents the so-called nucleation delay that is plotted against the corresponding particle temperature at the instance of nucleation in Figure 5 (left). The error bar for each point represents the spread of the nucleation time delay over the number of samples.

Note that even for spherical particles there is a measurable delay which is more pronounced at warmer nucleation temperatures. This is an indication of the significance of the kinetics of nucleation as the result of the nucleation energy barrier. To put this in context, for each 1 ms of nucleation delay, the particle would travel about 0.5 m in the exhaust plume. That being said, highly fractal particles ($D_f = 1.5$) could travel around 50 to 100 m downstream while remaining supercooled. This could have a substantial impact on the distance at which the contrail becomes visible, i.e., when it becomes optically thick.

An alternative analysis is to define a correlation between nucleation time delay and the cooling rate — an indication of how fast the temperature drops along a given particle trajectory. This correlation is shown in Figure 5 (right). The cooling rate values on the x -axis correspond to the temperature drop on the pathlines sampled in Figure 3, and the horizontal spread for each of the data points corresponds to the spread of the cooling rate over the sampled points. This figure seems to generally suggest that slower cooling rates and smaller fractal dimensions contribute to the larger nucleation delay.

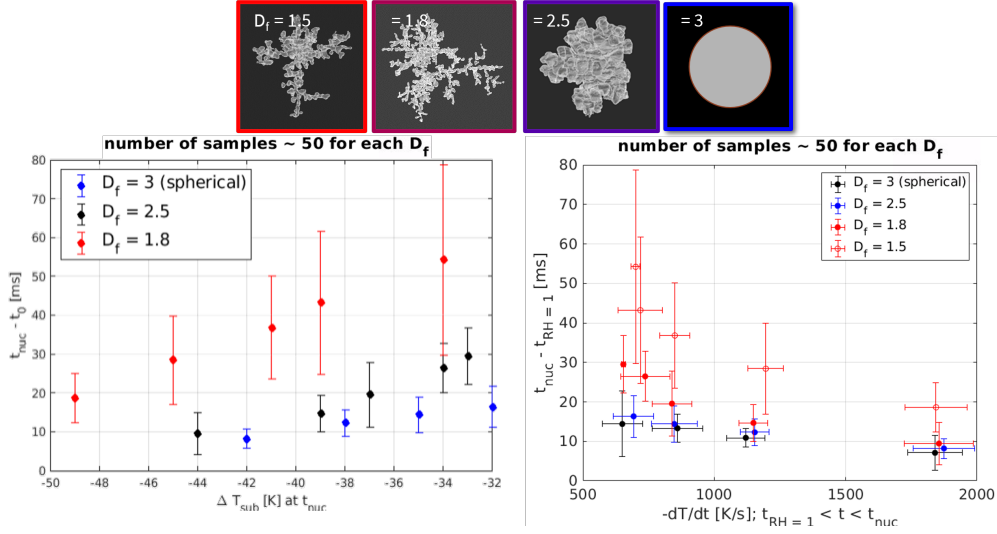


FIGURE 5. The top images visualize the fractal substrates developed under a soot growth model for the soot morphology study. The bottom graph shows the variation of nucleation delay, $t_{nuc} - t_0$ vs (left) the level of supercooling at the time of nucleation and (right) the cooling rate in the proximity of nucleation time.

4.2. Post-nucleation growth

In all the nucleation pathways presented above, the nucleus is a water embryo, meaning there is a condensation phase before ice nucleation occurs; this phase can take place either on the surface of the particle or within the water droplet. Post-nucleation growth consists of two stages: condensation and growth of the water droplet, which is driven by the interphase mass transfer from the ambient to the droplet. Freezing within the droplet is driven by bulk supercooled crystallization in an effectively infinite pool of supercooled water, whereas freezing in the ambient (initiated on the surface outside the droplet) is driven by thin-film crystallization. The fractal particles can go through the cooling process at a rate similar to that of the nucleation process, during which condensation and freezing rates are calculated.

Figure 6 shows an instantaneous snapshot of water and ice distribution around the particle for three fractal particles at different stages of growth. Interestingly, as the fractal dimension is reduced, the condensation droplet appears to evolve into a dimple-type configuration, typical of low-surface energy condensation. In addition, the freezing mechanism seems to evolve from primarily thin-film crystallization at higher fractal dimensions to what appears to be more bulk crystallization. This is counterintuitive to the nucleation findings in the preceding section and warrants more discussion.

Figure 7 shows the growth rate of condensate and crystal for two values of particle fractal dimension (solid lines). For both condensation and freezing, the growth rate seems to be augmented as the fractal dimension is reduced. For both mechanisms, it peaks at some intermediate time followed by a decline that is likely attributed to local heating as the result of phase-change heat release. The slowdown in the growth rate is expected for this reason. We hypothesize that the higher growth rate for lower fractal particles is likely due to a reduction in apparent surface energy of the particle—see Eq. (3.8). To test that hypothesis, similar particles are simulated but with a reduced surface energy (Figure 7,

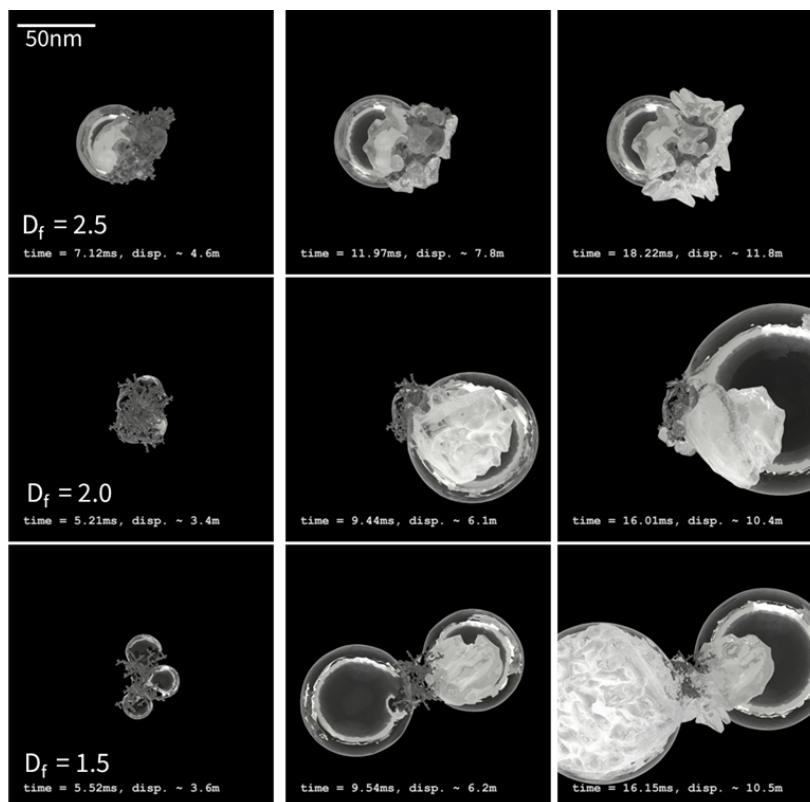


FIGURE 6. Instantaneous snapshots of simulation results for post-nucleation condensate and crystal growth for different fractal particles; $dT/dt \sim -1000 \text{ K s}^{-1}$.

dashed lines). The growth rate for both condensation and freezing is also augmented as the result of a reduction in particle surface energy. The likely explanation is that unlike a typical heterogeneous condensation and freezing, where the growth source is primarily supplied through heterogeneity (cold surface, for instance), the growth mechanism is sustained by a supersaturated ambient in this arrangement. As a result, when the surface energy of the particle decreases (either apparent surface energy due to lower fractal dimension or thermophysical surface energy due to the particle chemistry), the ice or water interface contact area with the surface is reduced, resulting in an increase in the corresponding exposed surface area, which enables an enhanced phase change across that interface. Both the fractal dimension parametric study and the thermophysical surface energy study seem to support this hypothesis, though a much more comprehensive study is needed to see if it is generally supported.

The implications of these findings can be quite significant. For instance, the conventional wisdom is that the nucleation on soot particles at the contrail's formation stage is assisted by them being coated with sulfuric acid or other volatile compounds that generally have more affinity to water than carbon (i.e., a higher surface energy). That conventional wisdom goes on to argue that as the result of that initial affinity, those particles are likely to remain inactive once ice and water eventually sublime and evaporate at the later stages of the contrail lifetime. The counterargument based on these findings is the following: the subsequent nucleation of the (now uncoated, and hence low-surface en-

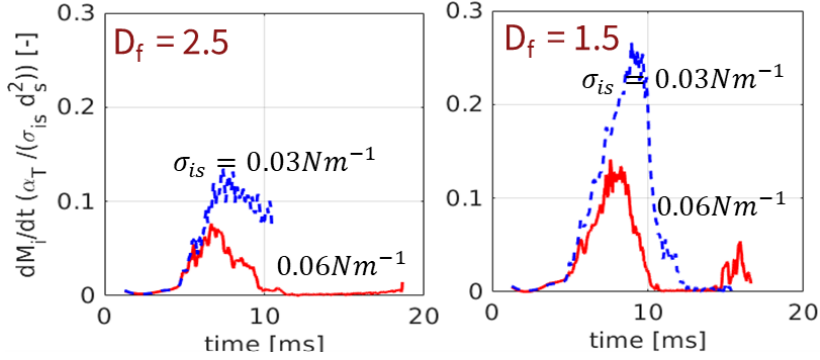


FIGURE 7. Calculated total growth rate for condensate and crystal for two fractal particles and two surface energies: $\sigma_{is} = 0.06 \text{ N m}^{-1}$ (red) and $\sigma_{is} = 0.03 \text{ N m}^{-1}$ (blue) nominally corresponding to sulfur coated carbon particles and uncoated particles, respectively.

ergy) particles does require more energy (read more supersaturation), which is supported by the nucleation study presented in Section 3.1. However, once they are activated, the nucleated ice and/or water could potentially grow more vigorously as the result of that much lower surface energy, resulting, potentially, in more ice and water content over the same period of time and for the same water availability. The implications for the ultimate optical properties of the eventual (cirrus) cloud are yet to be quantified.

5. Conclusion and future work

In this work, we investigated the role of soot morphology on the nucleation rates (condensation and freezing) and post-nucleation growth (condensational and depositional growth) of particles. Although an early stage study, preliminary results suggest that slower cooling rates and smaller fractal dimensions (as opposed to more spherical geometries) contribute to delay nucleation onset. However, the post-nucleation growth rate is enhanced as the fractal dimension is reduced. A plausible hypothesis for this behavior is dependence on the surface energy, but a more comprehensive study is necessary.

The present methodology can also be used to study the effect of the particle chemistry. This research would be especially meaningful, as different combustor designs (rich, lean and quench combinations) and types of fuel (kerosene, hydrogen and SAFs) impact, not only the soot particle morphology and chemistry but also the relevance of background aerosols in the formation of ice crystals. Extending this study to the field of atmospheric aerosols and/or volatile organic compounds would also be relevant to understanding the role of future alternative fuels on contrail mitigation.

Nevertheless, keep in mind that soot-induced ice crystals that do not fall out may remain at cruise altitudes for longer times and allow for secondary nucleation. Outcomes from this study point toward a higher barrier to renucleation, but the concerning part is that, if renucleation occurs, the rates of post-nucleation growth could lead to larger quantities of water and ice content in comparison with the original contrail. The challenging part, in terms of satellite detection, is that the now contrail cirrus cloud would most likely be indistinguishable from natural cirrus.

REFERENCES

- FRITZ, T. M. M. 2022 Plume to global-scale atmospheric impacts of aviation emissions. Ph.D. Thesis, Mass. Inst. of Technol.
- HARDT, S. & WONDRA, F. 2008 Evaporation model for interfacial flows based on a continuum-field representation of the source terms. *J. of Comput. Phys.* **227**, 5871–5895.
- KARMA, A. 2001 Phase-field formulation for quantitative modeling of alloy solidification. *Phys. Rev. Lett.* **87**, 115701.
- KULKARNI, G., CHINA, S., LIU, S., NANDASIRI, M., SHARMA, N., WILSON, J., AIKEN, A. C., CHAND, D., LASKIN, A., MAZZOLENI, C. *et al.* 2016 Ice nucleation activity of diesel soot particles at cirrus relevant temperature conditions: Effects of hydration, secondary organics coating, soot morphology, and coagulation. *Geophys. Res. Lett.* **43**, 3580–3588.
- LEE, D. S., FAHEY, D. W., SKOWRON, A., ALLEN, M. R., BURKHARDT, U., CHEN, Q., DOHERTY, S. J., FREEMAN, S., FORSTER, P. M., FUGLESTVEDT, J. *et al.* 2021 The contribution of global aviation to anthropogenic climate forcing for 2000 to 2018. *Atmos. Environ.* **244**, 117834.
- MINNIS, P., YOUNG, D. F., GARBER, D. P., NGUYEN, L., SMITH JR., W. L. & PALIKONDA, R. 1998 Transformation of contrails into cirrus during success. *Geophysical. Res. Lett.* **25**, 1157–1160.
- MITCHELL, P. & FRENKLACH, M. 1998 Monte Carlo simulation of soot aggregation with simultaneous surface growth—why primary particles appear spherical. In *Symp. (Int.) on Combust.*, , vol. 27, pp. 1507–1514. Amsterdam: Elsevier.
- NOGUERA, C., FRITZ, B., CLÉMENT, A. & BARONNET, A. 2006 Nucleation, growth and ageing scenarios in closed systems I: A unified mathematical framework for precipitation, condensation and crystallization. *J. of Crys. Growth* **297**, 180–186.
- SCHUMANN, U. 2012 A contrail cirrus prediction model. *Geosci. Model Dev.* **5**, 543–580.
- SLOWIK, J. G., CROSS, E. S., HAN, J.-H., DAVIDOVITS, P., ONASCH, T. B., JAYNE, J. T., WILLIAMS, L. R., CANAGARATNA, M. R., WORSNOP, D. R., CHAKRABARTY, R. K. *et al.* 2007 An inter-comparison of instruments measuring black carbon content of soot particles. *Aerosol Sci. Tech.* **41**, 295–314.
- VALI, G., DEMOTT, P., MÖHLER, O. & WHALE, T. 2015 A proposal for ice nucleation terminology. *Atmos. Chem. Phys.* **15**, 10263–10270.
- YAZDANI, M., HU, C. & MACDONALD, M. 2023 Icing simulation framework: A predictive approach from nucleation to runback. Tech. Rep. SAE Technical Paper.
- YAZDANI, M., RADCLIFF, T., SOTERIOU, M. & ALAHHARI, A. A. 2016 A high-fidelity approach towards simulation of pool boiling. *Phys. Fluids* **28**.